JACS
JOURNAL OF THE AMERICAN CHEMICAL SOCIETY

ARTICLE

pubs.acs.org/JACS

# Isomerization Mechanism in Hydrazone-Based Rotary Switches: Lateral Shift, Rotation, or Tautomerization?

Shainaz M. Landge,[†,∥] Ekatarina Tkatchouk,[‡] Diego Benítez,[‡] Don Antoine Lanfranchi,[§] Mourad Elhabiri,[§,⊥] William A. Goddard, III,[‡] and Ivan Aprahamian*[,†]

[†]Department of Chemistry, Dartmouth College, Hanover, New Hampshire 03755, United States

[‡]Materials and Process Simulation Center, California Institute of Technology, Pasadena, California 91125, United States

[§]Laboratoire de Chimie Bioorganique et Médicinale, Université de Strasbourg, ECPM, UMR 7509 CNRS-UdS, 25, rue Becquerel, 67200 Strasbourg, France

[⊥]Laboratoire de Physico-Chimie Bioinorganique, Université de Strasbourg, Institut de Chimie de Strasbourg, ECPM, UMR 7177 CNRS-UdS, 25, rue Becquerel, 67200 Strasbourg, France

[∥]Department of Chemistry, Georgia Southern University, Statesboro, Georgia 30458, United States

Supporting Information

**ABSTRACT:** Two intramolecularly hydrogen-bonded arylhydrazone (aryl = phenyl or naphthyl) molecular switches have been synthesized, and their full and reversible switching between the *E* and *Z* configurations have been demonstrated. These chemically controlled configurational rotary switches exist primarily as the *E* isomer at equilibrium and can be switched to the protonated *Z* configuration (**Z**-**H**$^+$) by the addition of trifluoroacetic acid. The protonation of the pyridine moiety in the switch induces a rotation around the hydrazone C═N double bond, leading to isomerization. Treating **Z**-**H**$^+$ with base ($K_2CO_3$) yields a mixture of *E* and "metastable" *Z* isomers. The latter thermally equilibrates to reinstate the initial isomer ratio. The rate of the *Z* → *E* isomerization process showed small changes as a function of solvent polarity, indicating that the isomerization might be going through the inversion mechanism (nonpolar transition state). However, the plot of the logarithm of the rate constant *k* vs the Dimroth parameter ($E_T$) gave a linear fit, demonstrating the involvement of a polar transition state (rotation mechanism). These two seemingly contradicting kinetic data were not enough to determine whether the isomerization mechanism goes through the rotation or inversion pathways. The highly negative entropy values obtained for both the forward (*E* → *Z*-H$^+$) and backward (*Z* → *E*) processes strongly suggest that the isomerization involves a polarized transition state that is highly organized (possibly involving a high degree of solvent organization), and hence it proceeds via a rotation mechanism as opposed to inversion. Computations of the *Z* ↔ *E* isomerization using density functional theory (DFT) at the M06/cc-pVTZ level and natural bond orbital (NBO) wave function analyses have shown that the favorable isomerization mechanism in these hydrogen-bonded systems is hydrazone−azo tautomerization followed by rotation around a C−N single bond, as opposed to the more common rotation mechanism around the C═N double bond.

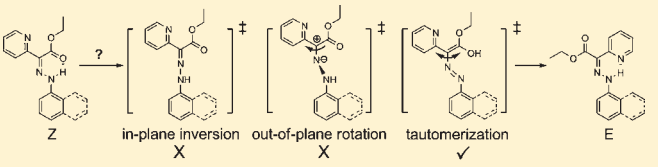


## INTRODUCTION

Molecular switches, motors and machines hold enormous promise for the advancement of nanotechnology.[1] The study and synthesis of such "smart" molecules that can mimic biological[2] and macroscopic counterparts has led to the development of a diverse array of molecular systems, such as switches,[3] shuttles,[4] muscles,[5] ratchets,[6] walkers,[7] robots,[8] memory devices,[9] etc., that can be activated using various external stimuli, e.g., chemical, electrochemical and photochemical. The induced motion can be rotary in nature or linear (translation) depending on the targeted application.[1] Synthetic rotary switches[10] are of particular interest as they resemble rotary motors found in nature (e.g., ATPases).[2] Such synthetic systems have given rise to the only known examples to date of synthetic motors that can undergo unidirectional motion.[11] These rotary systems undergo *conformational* changes when activated chemically, whereas photochemical modulation causes *configurational*[12] changes. There seems to be a significant lag in the area of chemically controlled *configurational* rotary switches and motors; bridging this gap may lead to novel functional systems and materials.[13]

The hydrazone functional group is versatile and has found extensive uses in medicine,[14] dynamic combinatorial chemistry (DCC),[15] foldamers,[16] and molecular tweezers,[17] to name a few. One important facet of hydrazone chemistry that has not been exploited thus far is the fact that upon appropriate substitution they can exist in solution as a mixture of isomers.[18] 1,2,3-Tricarbonyl-2-arylhydrazones (TCAHs)[19] for example can be

**Received:** January 24, 2011
**Published:** May 17, 2011





dx.doi.org/10.1021/ja200699v | *J. Am. Chem. Soc.* 2011, 133, 9812–9823

**Scheme 1. Possible Mechanism for the Acid-Catalyzed Tautomerization in TCAHs; Similar Scheme Can Be Drawn for the Base-Catalyzed Process**

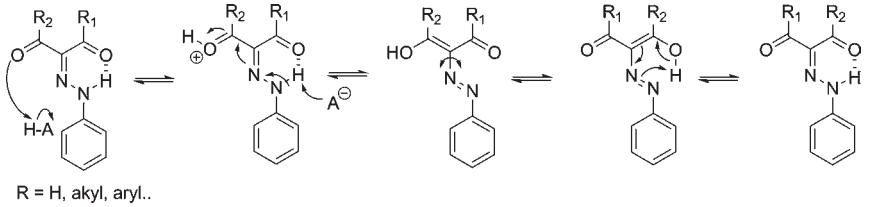


**Scheme 2. Mechanism of *E* ↔ *Z* Isomerization of Imines and Hydrazones**

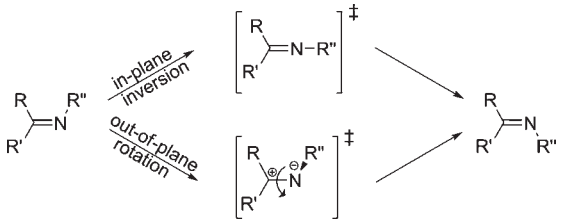


present in solution as a pair of intramolecularly H-bonded isomers (Scheme 1).[20] This H-bond causes a diagnostic low-field $^1$H NMR signal for the NH proton whose chemical shift depends on the type of carbonyl group to which it is attached. Hence, the different isomers can be readily distinguished using $^1$H NMR spectroscopy. TCAHs can be equilibrated in solution by the addition of a catalytic amount of acid or base (Scheme 1).[20] The isomerization mechanism in such instances consists of a hydrazone−azo tautomerization[21] followed by rotation around a C−N single bond that leads to a change in the relative position of the substituents around the C═N double bond (i.e., *E* → *Z* isomerization);[20d] however, this equilibration process is neither selective nor optimal and only affords a mixture of isomers (e.g., it can proceed from pure *E* to a mixture of *E* and *Z* isomers) that cannot be controllably switched back to the initial state.

The uncatalyzed isomerization around the C═N double bond (Scheme 2) is known[18,22] to proceed via two different mechanisms: rotation and inversion. The rotation mechanism proceeds through a polar transition state, and results in the rotation of the substituents around the C═N double bond. The inversion mechanism (also known as lateral shift) in contrast, occurs through an inversion around the imine nitrogen, and goes through a nonpolar transition state. Thus, the isomerization rates in the rotation mechanism show ***dependence*** on solvent polarity, whereas in the inversion mechanism no such effects are observed. This divergence in properties has been historically used in discerning the nature of the isomerization mechanism in various hydrazones and imines.

The isomerization mechanism has been studied in detail for imines,[23] and to a lesser extent for hydrazones,[24,25] and in both cases inversion is considered to be the common mechanistic pathway.[18,22,23,25] However, in most cases the studies focus on the ***rates of the isomerization process, and less attention is given to the contributions of enthalpy and entropy to the activation barrier; this can lead to misleading conclusions***, as attested by contradictory reports found in the literature.[26,27] These studies put the generality of the inversion mechanism into question.

**Scheme 3. Synthesis of 1 and 2**

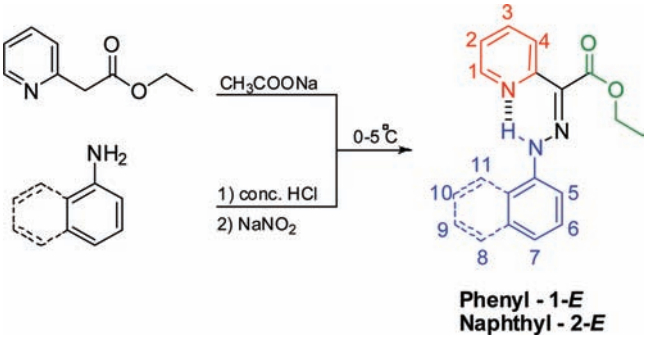


What is certain is that more experimentation needs to be conducted in order to fully understand the *E* ↔ *Z* isomerization mechanism in hydrazones, as this will eventually help us to finetune and control the switching process in arylhydrazone-based switches. Moreover, discerning the type of isomerization mechanism will be important as far as applications are concerned; the switching trajectory in each mechanism is different, rotation vs a pendulum-type motion (inversion), making each suitable for a different function.[1]

We have previously[28] shown that it is possible to convert the inefficient TCAH switches into reliable ones by replacing one of the carbonyl groups with a pyridine ring. Having a pyridine group as a proton acceptor and an ester moiety as a secondary H-bond acceptor attached to the imine carbon improved the control over the isomerization process. This structural change led to the bridging of the gap between *conformational* and *configurational* rotary switches and the development of chemically driven configurational rotary switches. Here we provide an experimental and computational account of the synthesis, characterization, pH switching,[29] and isomerization mechanism of two hydrazone-based rotary switches having different aryl stators; phenyl (**1**) and naphthyl (**2**).

## ■ RESULTS AND DISCUSSION

**Synthesis.** Compounds **1** and **2**[28a] were synthesized using a straightforward procedure (Scheme 3). First ethyl-2-pyridyl acetate was treated with sodium acetate in an ethanol−water mixture. In a second pot, the aromatic amine was treated with sodium nitrite and hydrochloric acid at 0 °C to create a diazonium salt. Both these solutions were mixed together at 0−5 °C and then brought to room temperature over a period of 1 h. The reaction mixture was stirred overnight during which the product precipitated out from the alcohol−water medium. The crude solid compound was then filtered from the mother liquor


dx.doi.org/10.1021/ja200699v | *J. Am. Chem. Soc.* 2011, 133, 9812–9823

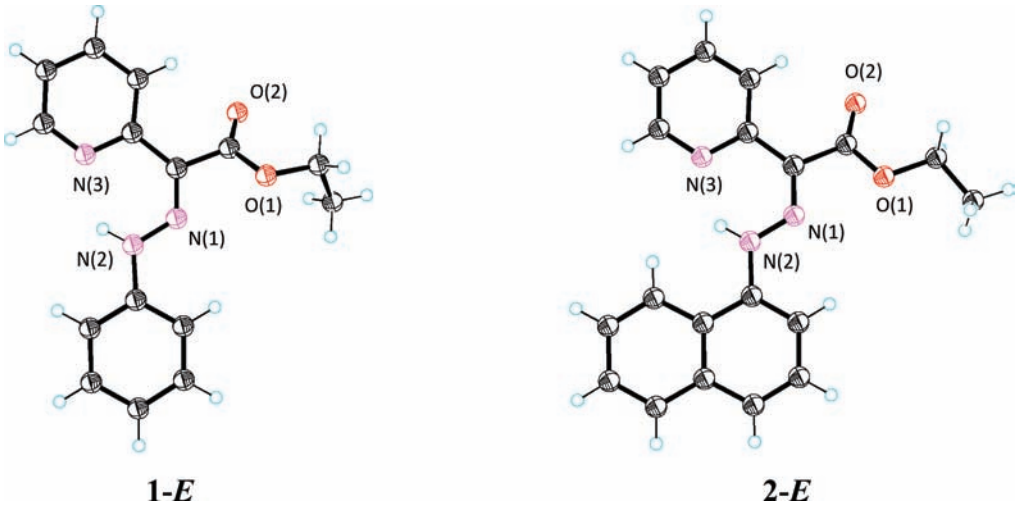


**Figure 1.** ORTEP drawing (50% probability ellipsoids) of **1**-*E* and **2**-*E*. The protons are placed in calculated positions, except for the hydrazone N(2)H proton.

and subjected to column chromatography ($SiO_2$, $CH_2Cl_2$/hexanes (1:2), respectively) to yield **1** (78%) and **2** (75%) as orange powders.

**Structural Characterization.** Crystals of the phenyl derivative (**1**) were obtained by slow evaporation of methanol, resulting in fine, orange needlelike crystals. A similar procedure using a mixture of $CH_2Cl_2$ and hexanes (1:1) resulted in the orange-red needlelike crystals of **2**. Both derivatives crystallize in the *E*-configuration (Figure 1).

The phenyl derivative (**1**-*E*) prefers to pack in a dimeric form, as seen across the *a*-axis (X-ray S1a in the Supporting Information [SI]) such that the ester oxygen of one molecule and the methyl protons of another are in close proximity with each other. We can see from the crystal structures (Figure 1) that there is an intramolecular H-bond (N−H···N: 1.997(1) Å, 130.88(10)° in **1**-*E* and 1.918(1) Å, 133.70(10)° in **2**-*E*) between the pyridine nitrogen (N3) and the hydrazone NH proton. It is also evident that in **2**-*E* the naphthalene bay area is oriented toward the NH hydrogen. The measured torsional angles[30] indicate that the systems are almost planar.[31] The comparison of the bond lengths[32] with those of similar intramolecularly H-bonded hydrazones (phenylhydrazone derivatives condensed with diesters),[33] leads us to conclude that the aryl rings are in conjugation with the pyridine and/or ester moieties. The intramolecular H-bond, the presence of a pseudo-six membered aromatic ring, and the $\pi$-delocalization all contribute to the planarity of the molecules.

The fully characterized $^1$H NMR spectrum of **1**-*E* in $CD_3CN$ (Figure 2, and Figure S1 in the SI) shows the presence of a distinct intramolecular H-bond between the pyridine nitrogen and the hydrazone proton. This H-bond manifests itself by a highly deshielded NH signal at 14.56 ppm. A small signal is also observed at 11.48 ppm stemming from the minor isomer, i.e., **1**-*Z*. The *E*:*Z* isomer ratio in $CD_3CN$ is 93:7 for **1** based on the integration of the NH signals. One-dimensional NOESY (Figure S2 in the SI) clearly shows that the pyridine is H-bonded with the hydrazone NH proton. The assigned structure in the solution phase agrees well with the solid-state structure. The H-bond between the pyridine and the hydrazone NH in **2**-*E* (Figure S3 in the SI) is evident by the signal resonating at 15.80 ppm. This proton is clearly affected by the naphthalene's ring current effect, as it resonates further downfield compared with **1**-*E*. One should also take into account the fact that the naphthyl group is a better electron-withdrawing group (EWG), making the NH proton more acidic, the H-bond stronger, and the structure more planar and hence more conjugated.[33] Moreover, resonance-assisted hydrogen bonding (RAHB)[34] comes into play in these systems, making the direct analysis of the difference in the chemical shift of the NH proton in **1**-*E* and **2**-*E* complicated. The $^1$H NMR spectrum of **2** also contains a small signal at 12.80 ppm stemming from **2**-*Z*. The isomer ratio for **2**, as deduced from integration, is 97:3 which is higher than in **1**. This slight difference in isomer ratio stems from the above-mentioned electronic effects that stabilize **2**-*E* more than **1**-*E*. One-dimensional (1D) NOESY (Figure S4 in the SI) clearly shows that the compound adopts the same rotameric form in solution as was observed in the solid state.[35]

**Computational Studies.** Both isomers of **1** and **2** were subjected to DFT calculations[36] at the M06/cc-pVTZ level.[37,38] The optimized geometries of both compounds predicted the *E* isomer to be more stable than *Z* in both acetonitrile and toluene as solvents. In the case of compound **1**, isomer *E* is $\Delta G^\circ$ = 1.2 kcal mol$^{-1}$ (1.5 kcal mol$^{-1}$ exp.) more stable than *Z*, whereas in **2**, isomer *E* is $\Delta G^\circ$ = 1.5 kcal mol$^{-1}$ (2.0 kcal mol$^{-1}$ exp.) more stable in acetonitrile as solvent. These data are in close agreement with the $^1$H NMR spectroscopy results. The calculations complement the X-ray structural analysis as they enable probing of the *Z* isomers, which could not be crystallized. The *Z* isomers of **1** and **2** deviate from planarity because of repulsion between the electron lone pairs on the imine and pyridine nitrogens (Figures Calc-S1 and Calc-S2 in the SI). A large torsion angle is present between the $N_{pyr}-C_{pyr}-C_{imin}=N$ atoms (37.3° for **1**-*Z* and 37.6° for **2**-*Z*) as compared to the planar *E* isomers (1.6° for **1**-*E* and 2.2° for **2**-*E*). The fact that the *Z* isomers are equally nonplanar supports the conclusion that the additional electronic stabilization of **2**-*E* (relative **1**-*E*) is the reason behind the slight difference in isomer ratio ($\Delta G^\circ$) observed in $CD_3CN$.

We also analyzed the NMR chemical shifts of **1** and **2** by comparing their calculated relative isotropic nuclear shieldings using the M06-L (no Hartree−Fock exchange) functional.[39] A comparison of the isotropic nuclear magnetic shielding constants for the hydrazone NH proton in a pair of rotamers of **2**-*E* (calculated 16.7 and 16.3 ppm, see SI for details) showed small

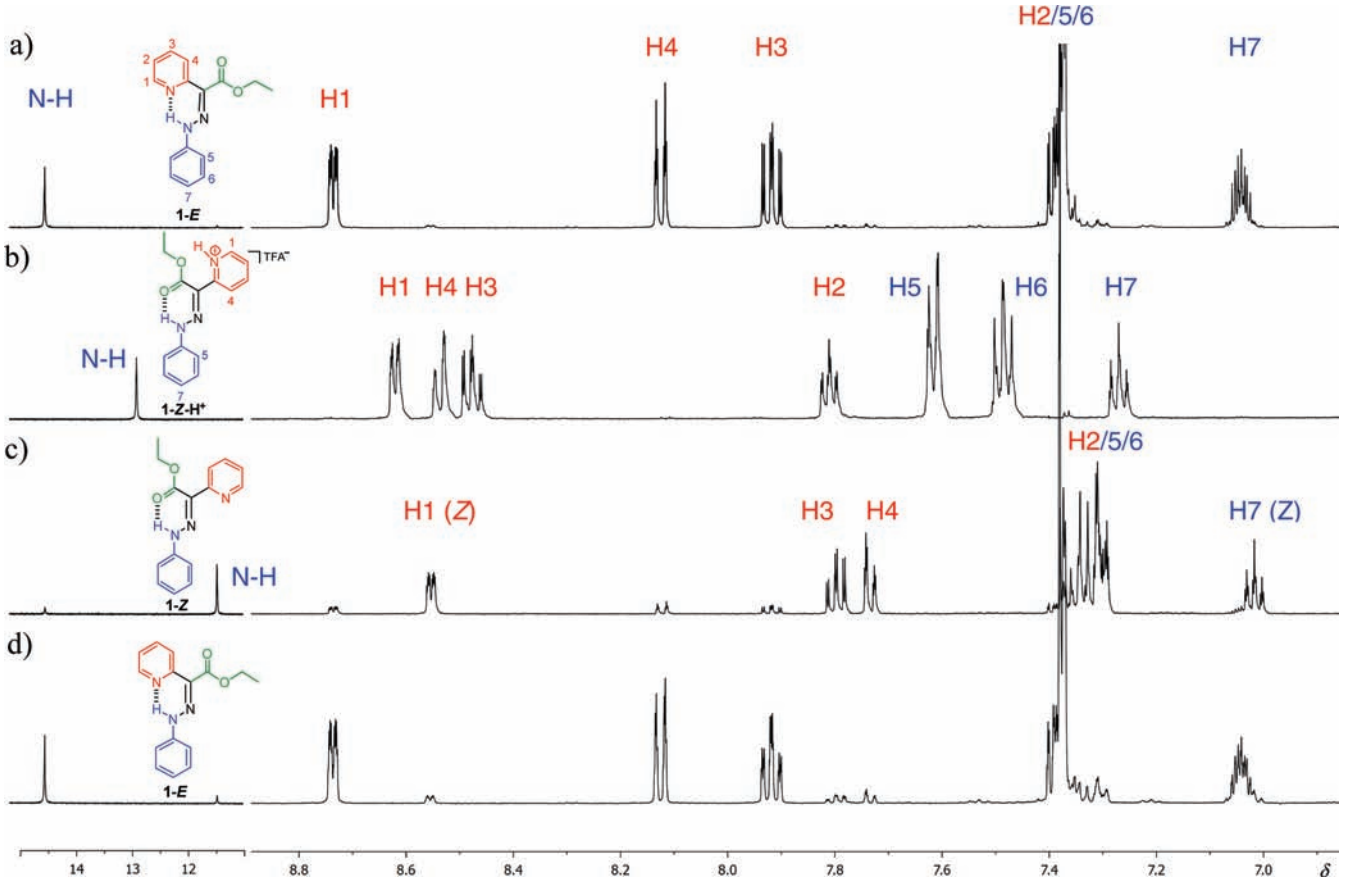


**Figure 2.** $^1$H NMR spectra (500 MHz) in $CD_3CN$ of (a) **1-*E*** with peak assignments; (b) **1-*Z*-H$^+$** with peak assignments, recorded after the addition of 2.2 equiv of TFA to **1-*E***; (c) a mixture of **1-*E*** and **1-*Z***, taken after passing **1-*Z*-H$^+$** over a plug of $K_2CO_3$; and (d) **1-*E*** after the mixture was left to equilibrate for 3 h at rt.

**Scheme 4. Acid/Base Controlled *E* ↔ *Z* Isomerization of 1**

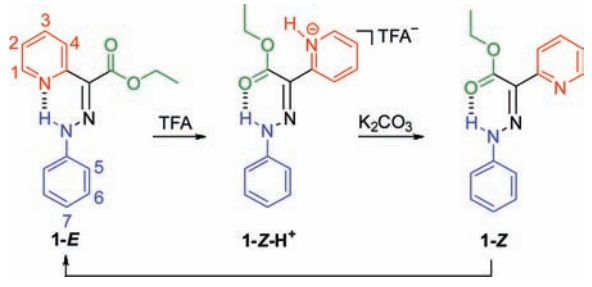


differences of only ~0.4 ppm between them. Our results suggest that the difference in the chemical shifts between **1** and **2** (exp. 14.6 and 15.8 ppm; calc. 15.6 and 16.7 ppm for the *E* isomers of **1** and **2**, respectively)[40] cannot be explained solely on the premise of ring current effect differences originating from both the relative orientation and the different aryl groups. RAHB[34] is definitely participating in determining the chemical shift of the NH protons.

*Acid–Base Switching Monitored by $^1$H NMR Spectroscopy.* The addition of 2.2 equiv of trifluoroacetic acid (TFA)[41] to a $CD_3CN$ solution **1-*E*** changes its color from light- to dark-yellow. It is expected that the protonation of the pyridine group in **1-*E*** will lead to breaking of the H-bond and rotation around the C═N double bond to form protonated **1-*Z*-H$^+$** (Scheme 4).

This process was monitored by $^1$H NMR spectroscopy; the addition of acid shifted the NH proton signal from 14.50 to 12.90 ppm (Figure 2b). This high-field shift indicates that the ester group is now H-bonded with the NH proton (**1-*Z*-H$^+$**).[20d] As expected the protonation also causes the pyridine protons to shift downfield.[42] Only proton H1 seems to move upfield (8.76 to 8.63 ppm) as it is no longer influenced by the H-bond and RAHB.[43] The phenyl protons also shift downfield, the most prevalent change being for proton H5 (from 7.38 to 7.62 ppm), indicating again that the pyridine ring is protonated. The 1D NOESY experiments (Figure S6 in the SI) show that the protonated pyridine nitrogen orients itself such that it is directed away from the phenyl ring. The color of the solution goes back to light-yellow when passed through a plug of potassium carbonate ($K_2CO_3$),[44] and a mixture of isomers is observed in the $^1$H NMR spectrum (Figure 2c). Distinct NH signals are observed at 11.48 and 14.56 ppm for the *Z* and *E* configurations, respectively. The "metastable" *Z* isomer thermally equilibrates with time to give back the more stable *E* isomer, showing the complete reversibility of the switching process (Figure 2d).

A similar process is observed when **2-*E*** is protonated.[28a] The addition of 2.0 equiv of TFA to **2-*E*** is accompanied by an upfield shift of the hydrazone NH proton from 15.8 to 13.9 ppm (Figure S7 in the SI). This shift indicates that the ester moiety is H-bonded with the NH proton (**2-*Z*-H$^+$**). The protonation causes the pyridine signals to shift downfield as expected. NOESY experiments indicate that the position of the naphthyl


dx.doi.org/10.1021/ja200699v | *J. Am. Chem. Soc.* 2011, 133, 9812–9823

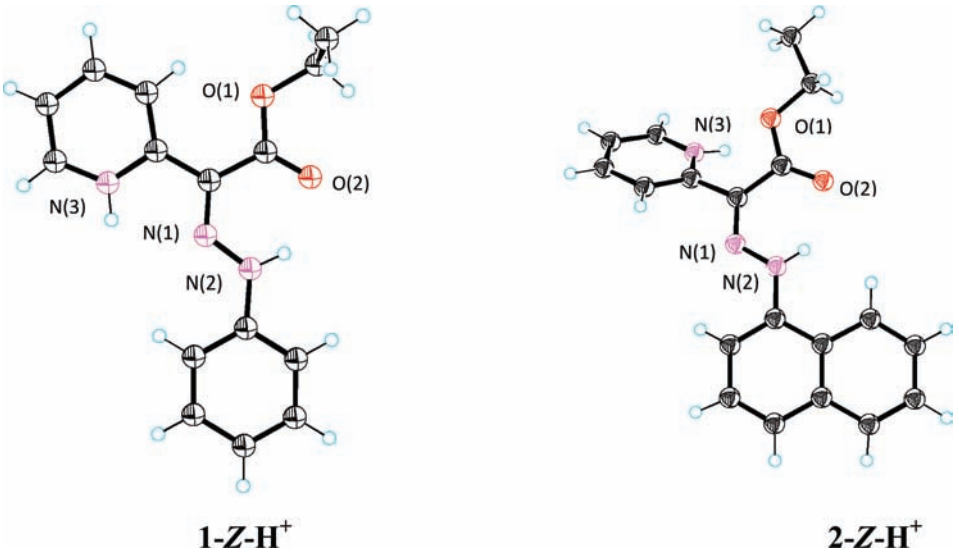


**Figure 3.** ORTEP drawing (50% probability ellipsoids) of **1**-*Z*-$H^+$ and **2**-*Z*-$H^+$. The protons are placed in calculated positions, except for the hydrazone N(2)H and N(3)H protons.

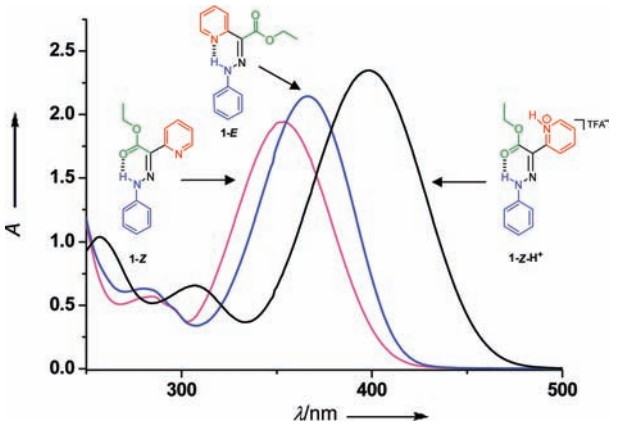


**Figure 4.** UV/vis spectra of the *E*, *Z* and *Z*-$H^+$ isomers of the phenyl-based molecular switch, **1**. All data were recorded in MeCN at 298 K.

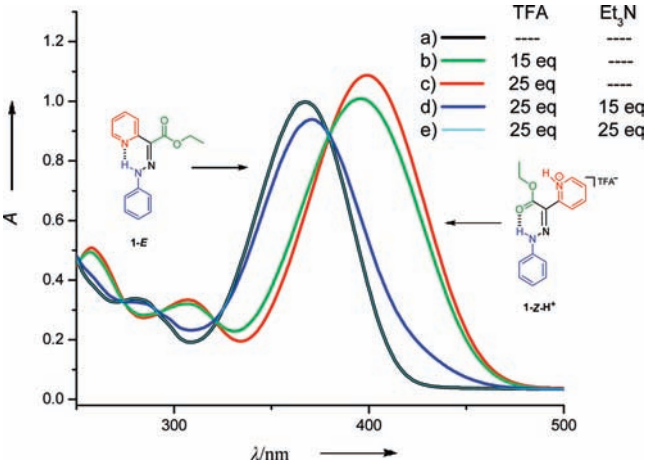


**Figure 5.** Changes in the UV/vis spectra during the acid/base switching of **1**-*E*. All data were recorded in MeCN at 298 K. To a $2.68 \times 10^{-5}$ M solution of **1**-*E* (a), was added TFA (b), until there was no observable change (c). $NEt_3$ was then added (d) to switch the system back (e). The signals of (a) and (e) are overlapping.

ring did not change as result of protonation (Figure S9 in the SI) and that the protonated pyridine nitrogen atom is oriented away from the naphthyl core (Figure S10 in the SI). After the solution is passed through a plug of $K_2CO_3$, two NH signals can be observed, one for the *E* isomer at 15.80 ppm and another for the *Z* isomer at 12.80 ppm. The *Z* isomer thermally equilibrates after a period of time to restore the original isomer ratio (97:3). This switching cycle with acid and base was repetitively demonstrated over five runs for both the naphthyl and phenyl derivatives with TFA as acid and triethylamine ($NEt_3$) as base.

The protonation of the pyridine ring was also confirmed by X-ray crystallography analysis (Figure 3). The structures of the protonated *Z* isomers, **1**-*Z*-$H^+$ and **2**-*Z*-$H^+$, clearly show that the intramolecular hydrogen bond (N−H···O: 1.905(1) Å, 133.00(10)° in **1**-*Z*-$H^+$ and 1.968(1) Å, 135.50(10)° in **2**-*Z*-$H^+$) is now between the ester carbonyl and the NH proton, in accordance with the NMR studies. Moreover, the naphthalene ring in **2**-*Z*-$H^+$ adopts the same rotameric form in the solid-state as observed in solution. The bond lengths and torsional angles[45] show that these systems are also fully conjugated and planar.

*Acid−Base Switching Monitored by UV/Vis Spectroscopy.* The complete switching cycles of compounds **1** and **2** were also fully characterized by UV/vis spectroscopy (Figures 4, 5, and S11−S16 in the SI). The *E* isomer of compounds **1** (Figure 4) and **2** (Figure S12 in the SI) is characterized by an intense and broad absorption band centered at $\lambda_{max}$ = 366 nm ($\varepsilon^{366} = 2.14 \times 10^4$ $M^{-1}$ $cm^{-1}$) and 392 nm ($\varepsilon^{392} = 1.96 \times 10^4$ $M^{-1}$ $cm^{-1}$), respectively. These bands result from the $\pi-\pi^*$ transitions of the aromatic units and are in agreement with the X-ray data that showed that the systems are fully conjugated. The extended aromatic unit in **2** leads to a bathochromic shift of 26 nm as compared to **1**. Both **1**-*E* and **2**-*E* possess weaker and almost isoabsorptive absorptions at higher energies as well (**1**-*E*: $\varepsilon^{280} = 6.33 \times 10^3$ $M^{-1}$ $cm^{-1}$ and **2**-*E*: $\varepsilon^{279} = 6.67 \times 10^3$ $M^{-1}$ $cm^{-1}$). The protonation of the pyridine subunit in these compounds (Figures 4 and S12 in SI), and the subsequent isomerization to the *Z*-$H^+$ isomers is supported by the bathochromic shift

**Table 1. Rate Constants and Gibbs Activation Energy Parameters for the $Z \leftrightarrow E$ Isomerization of 1 and 2 in Different Deuterated Solvents**

| | 1 | 2 |
|---|---|---|
| solvent ($E_T$) | $k$ ($\times 10^4$ s$^{-1}$) / $\Delta G^{\ddagger}$ (kcal mol$^{-1}$) | $k$ ($\times 10^4$ s$^{-1}$) / $\Delta G^{\ddagger}$ (kcal mol$^{-1}$) |
| toluene-$d_8$ (33.9) | $0.82 \pm 0.23/22.70 \pm 0.16$ | $0.57 \pm 0.21/22.90 \pm 0.21$ |
| $CDCl_3$ (39.1) | $1.76 \pm 0.11/22.30 \pm 0.03$ | $1.04 \pm 0.02/22.60 \pm 0.01$ |
| acetone-$d_6$ (42.2) | $3.34 \pm 0.26/21.90 \pm 0.04$ | $9.60 \pm 0.23/21.30 \pm 0.01$ |
| $CD_3CN$ (46) | $2.58 \pm 0.14/22.10 \pm 0.03$ | $3.54 \pm 0.04/21.80 \pm 0.01$ |

of ~32−34 nm in the main absorption band (**1**-*Z*-**H**$^+$: $\varepsilon^{398} = 2.35 \times 10^4$ M$^{-1}$ cm$^{-1}$ and **2**-*Z*-**H**$^+$: $\varepsilon^{426} = 1.94 \times 10^4$ M$^{-1}$ cm$^{-1}$). The deprotonation of the *Z*-**H**$^+$ isomers using $NEt_3$ leads to the "metastable" *Z* isomers, which is accompanied by a strong hypsochromic shift of ~46 nm of the main absorption band (**1**-*Z*: $\varepsilon^{352} = 1.94 \times 10^4$ M$^{-1}$ cm$^{-1}$ and **2**-*Z*: $\varepsilon^{380} = 1.75 \times 10^4$ M$^{-1}$ cm$^{-1}$).[46]

The reversibility of the switching process was demonstrated by UV/vis spectroscopy as well (Figures 5 and S11 in SI). The absorption maximum of **1**-*E* at $\lambda_{max} = 366$ nm (Figure 5a) shifts bathochromicly to $\lambda_{max} = 392$ nm (Figure 5c) when titrated with TFA (25 equiv). New peaks emerge at $\lambda = 307$ ($\varepsilon^{307} = 6.57 \times 10^3$ M$^{-1}$ cm$^{-1}$) and 257 nm ($\varepsilon^{257} = 1.04 \times 10^4$ M$^{-1}$ cm$^{-1}$) in the protonated form. When **1**-*Z*-**H**$^+$ is titrated with $NEt_3$ (Figure 5d) the original absorption is regenerated (Figure 5d). Four isosbestic points were visible during the entire switching cycle at $\lambda = 274$, 292, 320, and 379 nm (Figure S11 in the SI) showing that only two species are involved in the process.[47] A similar behavior is also observed for the naphthyl derivative (Figures S12−14 in the SI); the absorption of **2**-*E* at $\lambda_{max} = 392$ nm, is shifted to $\lambda_{max} = 426$ nm upon protonation with TFA (Figure S13c in SI). Four isosbestic points are observed at $\lambda = 241$, 264, 339, and 408 nm during this process. Treating **2**-*Z*-**H**$^+$ with excess of $NEt_3$ restores the original spectrum (Figure S13e in SI), attesting to the reversibility of the switching process. These acid−base switching cycles can be reversibly repeated multiple times for both **1** and **2**.

**Mechanistic Studies: Computation, Kinetics and Thermodynamics.** *NMR Analysis.* In order to gain insight into the switching mechanism of the H-bonded arylhydrazone switches, we first performed a thorough study of the $Z \rightarrow E$ thermal equilibration using $^1$H NMR spectroscopy. The rate of equilibration was studied by following the changes in the intensity of the NH signal of the *Z* configuration as a function of time. The rate constants ($k$) were then calculated from nonlinear least-squares fittings and the Gibbs energy of activation ($\Delta G^{\ddagger}$) was calculated using the Eyring equation.[48] The initial equilibrium ratio was taken into account when performing these calculations and only the contribution of $k_{Z\rightarrow E}$ (referred to as $k$ from now on) to the measured rates was used in determining the different kinetic and thermodynamic parameters (see SI for more details).[49]

The rate measurements were conducted multiple times at room temperature (Figure S17 in SI) in different solvents having various polarities (Table 1): $CD_3CN$, acetone-$d_6$, $CDCl_3$ and toluene-$d_8$. It was observed that the isomerization rate increases and the $\Delta G_{298}^{\ddagger}$ value decreases when going from the nonpolar to the more polar solvents. The difference in the rate between the extremities, toluene-$d_8$ and $CD_3CN$, is 6.2 times for **2** and 3.1 times for **1**.[50] In acetone-$d_6$ the rates are slightly higher than in $CD_3CN$ and this might be explained by the fact that a higher concentration of TFA is required (~18 vs 2 equiv) to protonate the system in acetone, which can change the ionic strength of the solvent. Moreover, it has been reported in the literature that acetone can form hydrogen bonds with the acidic NH proton,[25e] which can affect the isomerization rate. The differences in rate constants when changing the polarity of the solvent are not substantial, and when compared with reported results[25] one might conclude that the isomerization process goes through the lateral inversion mechanism. However, both derivatives show a linear relationship between log $k$ and the Dimroth parameter ($E_T$)[51] (Figure S18 in the SI), which is a clear indication for the involvement of a polarized transition state in the process.

*Mechanism Calculations.* In order to gain further insight into the isomerization mechanism of **1** and **2** we performed calculations on the possible pathways including inversion and different flavors of rotation. The inversion pathway happens through a change in the hybridization of the N atom; from $sp^2$ to sp at the linear transition state. The $sp^2$ lone pair changes to a transitory filled p orbital to allow the inversion to occur. Using the M06 functional,[37] we calculated a barrier to inversion of 67.0 kcal/mol for **1**. This process exhibits a predicted barrier for the *Z* to *E* transformation that is not consistent with the experimental observations.

The rotation mechanism can occur via several pathways, depending on the reorganization of the electrons participating in the C=N $\pi$-bond: heterolysis, homolysis, and tautomerization. Heterolysis of the C=N bond produces a zwitterionic transition state, while the homolysis produces a triplet intermediate. We performed calculations using the M06 functional on the singlet state rotation that leads to a charge separated transition state. Our computational methodology (M06/cc-pVTZ)[37,38] predicts a barrier of 55.6 kcal/mol for the heterolytic rotation around the C=N bond of **1** in acetonitrile, also not consistent with the experimental observations.

Homolysis leads to a stable triplet intermediate where the dihedral $C_{pyr}-C=N-N$ is 90°. Therefore, in principle, the potential energy surface for the rotation process follows the singlet energy valley at low dihedral angles and the triplet energy valley at high dihedral angles. We estimate the crossover point around ~60° from relaxed coordinate scans for both the singlet state and the triplet state. We calculated that the barrier for the homolytic rotation is at least 42.7 kcal/mol for **1** in acetonitrile, which is not consistent with our experiments.

We also considered a mechanism where a hydrazone−azo tautomerization reorganizes the $\pi$-electronic framework along the extended delocalized system (Figure 6), thus enabling rotation around a C−N single bond. Several reports have proposed such an isomerization mechanism in TCAHs when using acid/base catalysts;[20d] however, such an isomerization has not been considered thus far as a viable pathway in the absence of a catalyst.[52] We believe that the pyridyl group (significantly more basic than the carbonyl) greatly favors proton exchange and acts as an internal "catalyst". We envision a mechanism where the isomerization proceeds via a rotational transition structure that has an azo form with a dihedral angle $C_{pyr}-C_{imin}-N-N$ (and $C_{ester}-C_{imin}-N-N$) at ~90°. This is in contrast to a triplet state (from homolysis) that would exhibit pyramidalization (from rehybridization) of the $C_{imin}$ atom. We calculated the barrier for such a tautomerization and found it to be 23.8 and 24.3 kcal/mol for **1** and **2**, respectively, in acetonitrile. The magnitude of these barriers is consistent with our experimental data (Table 1).[53]

We further characterized **1**-*E* and **2**-*E*, as well as **1TS** and **2TS**, using natural bond orbital (NBO) formalism and software[54]

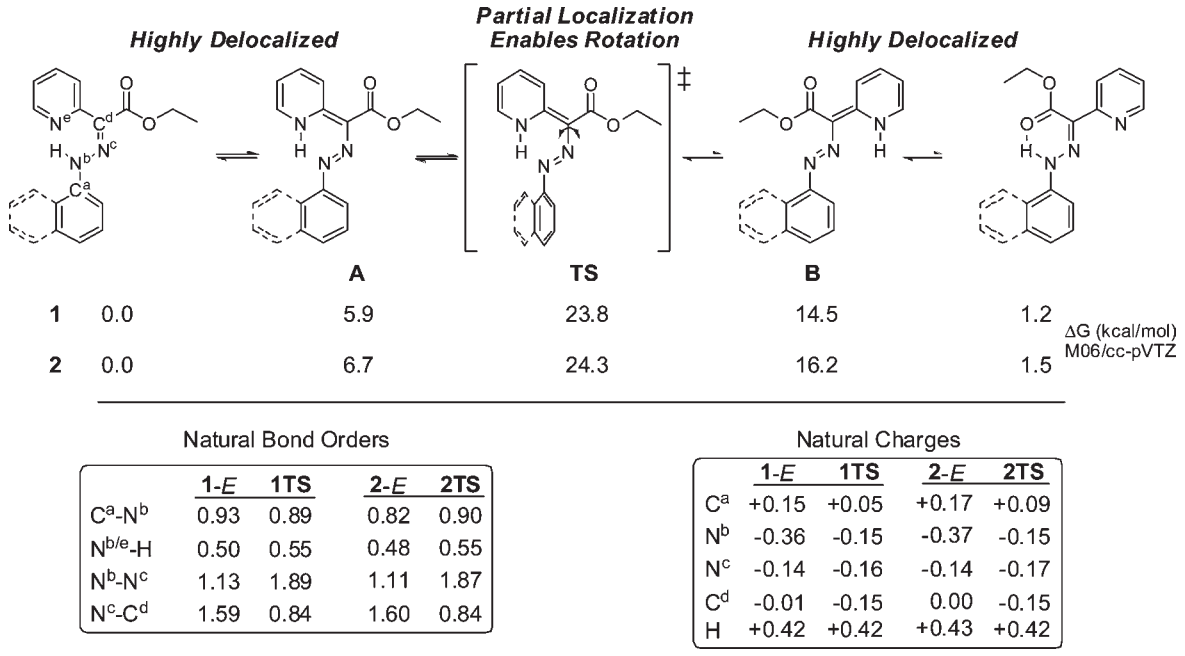


Natural Bond Orders

| | 1-*E* | 1TS | 2-*E* | 2TS |
|---|---|---|---|---|
| $C^a$-$N^b$ | 0.93 | 0.89 | 0.82 | 0.90 |
| $N^{b/e}$-H | 0.50 | 0.55 | 0.48 | 0.55 |
| $N^b$-$N^c$ | 1.13 | 1.89 | 1.11 | 1.87 |
| $N^c$-$C^d$ | 1.59 | 0.84 | 1.60 | 0.84 |

Natural Charges

| | 1-*E* | 1TS | 2-*E* | 2TS |
|---|---|---|---|---|
| $C^a$ | +0.15 | +0.05 | +0.17 | +0.09 |
| $N^b$ | -0.36 | -0.15 | -0.37 | -0.15 |
| $N^c$ | -0.14 | -0.16 | -0.14 | -0.17 |
| $C^d$ | -0.01 | -0.15 | 0.00 | -0.15 |
| H | +0.42 | +0.42 | +0.43 | +0.42 |

**Figure 6.** Potential free energy (M06/cc-pVTZ) landscape for the proposed intermediates and transition structure for the rotational isomerization process of switches **1** and **2** in acetonitrile. Selected natural bond orders and charges from natural localized molecular orbitals and natural populations for structures **1**-*E*, **2**-*E*, **1TS**, and **2TS**.

**Table 2. Activation Parameters for the $Z \leftrightarrow E$ Isomerization of 1 and 2 in Toluene-$d_8$ and $CD_3CN$**

| molecular switch (solvent) | $E_a$ (kcal mol$^{-1}$) | $\Delta H^{\ddagger}$ (kcal mol$^{-1}$) | $T\Delta S^{\ddagger}$ (kcal mol$^{-1}$) | $\Delta S^{\ddagger}$ (cal mol$^{-1}$ K$^{-1}$) |
|---|---|---|---|---|
| **1** (toluene-$d_8$) | 6.7 ± 1.1 | 6.1 ± 1.1 | −16.7 ± 0.2 | −56.6 ± 3.7 |
| **2** (toluene-$d_8$) | 8.3 ± 1.3 | 7.7 ± 1.3 | −15.2 ± 0.2 | −51.9 ± 4.5 |
| **1** ($CD_3CN$) | 9.6 ± 0.4 | 9.0 ± 0.4 | −13.1 ± 0.1 | −44.5 ± 1.4 |
| **2** ($CD_3CN$) | 11.2 ± 0.7 | 10.6 ± 0.7 | −11.2 ± 0.1 | −38.0 ± 2.3 |

(Figure 6). Compounds **1**-*E* and **2**-*E* exhibit a highly delocalized $\pi$-electron system. In contrast, in compounds **1TS** and **2TS**, the $\pi$-system of the N atoms and terminal aryl (phenyl in **1** or naphthyl in **2**) lie orthogonal to the pyridyl-ester $\pi$-orbitals. This renders the electronics in both transition structures almost identical. However, the different aryl groups—phenyl or naphthyl—have marked effects on the electronics of **1**-*E* and **2**-*E*. This is exhibited by the change in the bond order between $C^a$ and $N^b$ from **1**-*E* to **1TS** and from **2**-*E* to **2TS** (Figure 6). For the case of phenyl (**1**), the $C^a$—$N^b$ natural bond order decreases from 0.93 to 0.89, while the same bond order increases from 0.82 to 0.90 for naphthyl (**2**). These differences are also reflected (albeit to a minor degree) in the neighboring bonds, which are more relevant to the rotational barrier. These data suggest that the difference in the barriers to rotation in **1** and **2** is associated with the partial localization of the $\pi$-electron system from the highly delocalized ground state to the less delocalized transition state. Furthermore, we calculated the dipole moments for the wave functions of structrues **1**-*E*, **1TS**, **2**-*E* and **2TS** in a dielectric continuum for acetonitrile. We found that the ground states have a much smaller dipole moment: 2.7 and 3.0 D for **1**-*E* and **2**-*E*, respectively, while the transition states exhibit a much higher dipole moment: 6.8 and 6.7 D for **1TS** and **2TS,** respectively (Figures Calc-S3 and Calc-S4 in the SI). This is in agreement with our experimental determination of the dependence of the isomerization rates on solvent polarity, which suggests that the rate-determining step involves a more polar transition structure.

*Thermodynamic Parameters.* Relying solely on the changes in rate constant (and subsequently the Gibbs energy of activation)[27] as a function of solvent polarity cannot be used as the only basis to support the isomerization mechanism in these H-bonded arylhydrazones. In order to reach a better conclusion about the mechanism, one has to look at the full picture, which entails a full analysis of not only the rates of the process but also the contribution of the entropy and enthalpy parameters. To accomplish this we extended the rate constant measurement studies in toluene-$d_8$ and $CD_3CN$ to a range of temperatures: 294.5−338.5 K for toluene-$d_8$ and 268.5−308.5 K for $CD_3CN$. In toluene-$d_8$ (Table S1 in the SI) the rates are almost the same for **1** and **2** over the range of temperatures, whereas in $CD_3CN$ the rates are consistently higher for **2** (Table S2 in the SI). These data were applied in calculating (Table 2) the enthalpy of activation ($\Delta H^{\ddagger}$), entropy of activation ($\Delta S^{\ddagger}$), and energy of activation ($E_a$) using the Eyring and Arrhenius equations (Figures S19−20 in the SI). The large negative $\Delta S^{\ddagger}$ value of both systems regardless of the solvent can be interpreted as *further evidence for the involvement of a polarized transition state* in the isomerization process, given that at the rate-determining step, solvent molecules may associate to solvate the more polar transition structure. This parameter is less negative in more polar $CD_3CN$, which requires less reorganization to stabilize the polar transition state.


dx.doi.org/10.1021/ja200699v | *J. Am. Chem. Soc.* 2011, 133, 9812–9823

Table 3. Kinetic Data and Activation Parameters for the *E* to *Z*-H$^+$ Isomerization of 1 and 2 in $CH_3CN$

| molecular switch | $k_{E\rightarrow Z}$[a] ( $\times 10^{-2}$ $s^{-1}$) | $E_a$ (kcal $mol^{-1}$) | $\Delta H^{\ddagger}$ (kcal $mol^{-1}$) | $T\Delta S^{\ddagger}$ (kcal $mol^{-1}$) | $\Delta S^{\ddagger}$ (cal $mol^{-1}$ $K^{-1}$) |
|---|---|---|---|---|---|
| **1** | 2.7 ± 0.3 | 15.6 ± 0.5 | 15.1 ± 0.5 | −4.70 ± 0.05 | −15.8 ± 1.9 |
| **2** | 5.2 ± 0.3 | 16.3 ± 0.7 | 15.8 ± 0.7 | −3.6 ± 0.5 | −11.5 ± 1.7 |

[a] Determined at 25.0(2) °C.

When comparing **1** and **2**, it is evident that the electronics of the aryl group affect the transition state.The naphthyl group is a better EWG and can better stabilize the polarized transition state, thus requiring less solvent reorganization and resulting in a less negative $\Delta S^{\ddagger}$ value. On the other hand the naphthyl group makes the NH proton more acidic and hence the H-bond with the ester carbonyl is stronger as manifested in the larger $\Delta H^{\ddagger}$ and $E_a$ values. The H-bond has to be broken first in order for the isomerization to proceed, and this explains the positive enthalpy values for both switches. These two opposing effects cause the isomerization rates of **1** and **2** to be almost the same in toluene-$d_8$. In $CD_3CN$, the $\Delta H^{\ddagger}$ and $E_a$ values are larger than in toluene-$d_8$ because of the solvent's promotion of H-bonding; however, the change for both systems is almost the same ($\Delta\Delta H^{\ddagger}$ is 2.9 and 3.0 kcal $mol^{-1}$, for **1** and **2**, respectively). The same holds true for the $E_a$ values. Conversely, the stabilization of the transition state is larger in **2** compared to **1** ($\Delta\Delta S^{\ddagger}$ is 13.9 and 12.1 cal $mol^{-1}$ $K^{-1}$, respectively), which results in the 0.3 kcal $mol^{-1}$ difference in the $\Delta G^{\ddagger}$ value (Table 1) between **1** and **2** in $CD_3CN$, and the rate differences between them when going from the less polar to the more polar solvent. Overall, the opposing contributions of enthalpy and entropy result in the observed small dependence of isomerization rate on solvent polarity.

*UV/Vis Analysis.* The *E* → *Z*-H$^+$ isomerizations of compounds **1** and **2** were probed in $CH_3CN$ using a stopped flow spectrophotometer (Figures S21 and S22 in SI). The isomerization was easily monitored because of significant spectral variations induced by the protonation of the pyridine unit and by the subsequent switching of the corresponding molecules. Kinetic measurements were carried out under pseudo-first-order conditions ($[TFA]_{tot} \geq 10 \times [\mathbf{1}]_{tot}$ or $[\mathbf{2}]_{tot}$). In all cases, a single-exponential signal versus time (Figures S21 and S22 in the SI) was recorded when monitoring the main $\pi-\pi^*$ absorption band at 409 and 450 nm for **1** and **2**, respectively. These two wavelengths were chosen because they correspond to the maximum spectral amplitude difference between the reactants and the products. The mono-exponential nature of the recorded kinetic signal indicates a first-order reaction kinetics with respect to **1** or **2**. The absorbance values measured at the beginning and at the end of the experimental kinetic traces were found to be in agreement with the values expected from the measurements performed at equilibrium. These results show that there are no additional fast or slow steps that might be lost while mixing the reagents (~3 ms). The $[TFA]_{tot}$ was varied, and the average pseudo-first-order rate constants ($k_{obs}$) were determined (see SI for more details).[55] The variations of the corresponding $k_{obs}$ with $[TFA]_{tot}$ are given in Figures S21 and S22 in the SI and obey the following relationship:[56]

$$k_{obs} = \frac{a[TFA]_{tot}}{1 + b[TFA]_{tot}} + c$$

where $a = k_{EH^+\rightarrow ZH^+} \times K_H$, $b = K_H$ and $c = k_{ZH^+\rightarrow EH^+}$

The *E* → *Z*-H$^+$ reaction is triggered only when the pyridine is protonated. This acid−base reaction is extremely fast and reaches equilibrium within the mixing time of the stopped-flow apparatus (~3 ms). It can be therefore considered as a fast pre-equilibrium affording the *E*-H$^+$ kinetic intermediate. The rate-limiting step therefore corresponds to the *E*H$^+$ → *Z*H$^+$ isomerization that can be described as follows:

$$E \overset{K_H}{\rightleftarrows} E\text{-}H^{+*} \quad \text{fast pre-equilibrium}$$

$$E\text{-}H^{+*} \overset{k_{E/Z}}{\rightarrow} Z\text{-}H^{+} \quad \text{rate-limiting step}$$

Nonlinear least-squares fittings of the variations of $k_{obs}$ versus $[TFA]_{tot}$ allowed us to determine the monomolecular rate constant $k_{EH+\rightarrow ZH+}$ (referred to as $k_{E\rightarrow Z}$ from now on for the sake of simplicity) of the *E* → *Z*-H$^+$ isomerization process (Table 3). Interestingly, the first order isomerization rate constant $k_{E\rightarrow Z}$ calculated for the naphthyl derivative **2** ($k_{E\rightarrow Z}$ = 5.2(3) × $10^{-2}$ $s^{-1}$) is about 2 times higher than that of **1** ($k_{E\rightarrow Z}$ = 2.7(3) × $10^{-2}$ $s^{-1}$). As previously discussed, this feature supports the involvement of a polarized transition state in the isomerization process. The more extended naphthyl $\pi$-system stabilizes the transition state of **2** better than in **1**, and hence, the reaction goes faster.

The activation parameters for the *E* → *Z*-H$^+$ isomerization process (Table 3) in $CH_3CN$ have been determined as well using the $k_{E\rightarrow Z}$ rates (Figures S23 and S24 in the SI). As stated earlier, the rather large negative $\Delta S^{\ddagger}$ value for both systems is evidence for the rotation mechanism.[24] The lesser negative values measured for the *E* → *Z*-H$^+$ isomerization process with respect to the thermal *Z* → *E* one indicate that there are fewer reorganization constraints for the stabilization of the polar transition state. This may be explained by the fact that the H-bond within the *E*-H$^+$ kinetic intermediates has been already disrupted because of the protonation of the pyridine moiety. One also has to take into account the fact that the polarity and ionic strength of $CH_3CN$ might have been altered as a result of the addition of more than 100 equiv of TFA to the solution (See experimental details in the SI). When comparing the entropies of activation ($\Delta S^{\ddagger}$ = −15.8(1.9) cal $mol^{-1}$ $K^{-1}$ for **1** and $\Delta S^{\ddagger}$ = −11.5(1.7) cal $mol^{-1}$ $K^{-1}$ for **2**) it becomes clear that **2** has a more stabilized transition state as a result of its extended $\pi$-system. The $\Delta H^{\ddagger}$ and $E_a$ values measured for **1** and **2** (Table 3) were found to be within the error range, which is in agreement with the fact that in the *E*-H$^+$ kinetic intermediates, the H-bonds have been already dissociated.

On the basis of the kinetic and thermodynamic studies we can conclude that both the *E*-H$^+$ ↔ *Z*-H$^+$ and the *Z* ↔ *E* isomerization processes in these H-bonded arylhydrazone switches go through a polar transition state. When we couple these results with our computational studies we can conclude that the isomerization mechanism involves hydrazone−azo tautomerization followed by rotation around a C−N single bond (Figure 6), and not the standard rotation around a C═N double bond (Scheme 2). If we were to only consider the rate data, we would have come to the wrong conclusion, as it happened with others before us.[27]

**The Catalyzing Effect of $NEt_3$ on the *Z*-H$^+$→*E* Isomerization Process.** We also examined the kinetics of the *Z*-H$^+$ → *E* isomerization process using UV/vis spectroscopy (Figures S25

and S26 in the SI). Pseudo-first-order conditions ($[NEt_3]_{tot} \geq 10 \times [\mathbf{1}\text{-}\mathbf{Z}\text{-}\mathbf{H}^+]_{tot}$ or $[\mathbf{2}\text{-}\mathbf{Z}\text{-}\mathbf{H}^+]_{tot}$) were used for these measurements as well. The "metastable" *Z* isomer of both compounds **1** and **2**, obtained from the deprotonation of the *Z*-$H^+$ isomer could be characterized spectrophotometrically (Figure 4 and Figure S11 in the SI). A strong hypsochromic shift of about 46 nm was observed upon deprotonation of the pyridinium unit, and a single rate-limiting step subsequent to this protolytic equilibrium was measured that was assigned to the $Z \rightarrow E$ isomerization reaction. The latter process was accompanied by bathochromic ($\Delta\lambda \approx 12-14$ nm) and hyperchromic shifts that eventually afforded absorption spectra that entirely matched those of **1**-*E* or **2**-*E*. The $[NEt_3]_{tot}$ were varied, and the average pseudo-first-order rate constants ($k_{obs}$) were determined.[55] The corresponding $k_{obs}$ linearly varies with $[NEt_3]_{tot}$ with a significant intercept at the origin. As we discussed earlier, base can be used to catalyze the equilibration process in TCAHs (Scheme 1).[20] We can therefore rationalize our kinetic data by assuming a similar catalyzing influence of the $NEt_3$ base on the $Z \rightarrow E$ isomerization process. This actually can explain why during our NMR studies we barely saw the *Z* isomer when we deprotonated the *Z*-$H^+$ one by adding $NEt_3$ to the NMR tube.[44] The statistical processing of the kinetic data allowed for the determination of the second-order rate constants $k_{NEt3}$ ($M^{-1}$ $s^{-1}$) that correspond to the bimolecular $Z \rightarrow E$ isomerization pathway with catalysis by $NEt_3$ for **1** ($k_{NEt3} = 1.0 \pm 0.1\ M^{-1}\ s^{-1}$) and **2** ($k_{NEt3} = 7.2 \pm 0.8\ M^{-1}\ s^{-1}$). The intercept at the origin is assumed to correspond to the first-order rate constant for the uncatalyzed pathway and was found to be equal to $k_{Z\rightarrow E} = 2.1 \pm 0.9 \times 10^{-3}\ s^{-1}$ for **1** and $k_{Z\rightarrow E} = 3.7 \pm 0.3 \times 10^{-3}\ s^{-1}$ for **2** under our experimental conditions. It is noteworthy that these values are about 1 order of magnitude higher than those obtained by $^1H$ NMR spectroscopy studies (Table 1). This discrepancy can be easily explained if one takes into account the fact that in the UV/vis spectroscopy studies the solutions contained large excess of the salt $Et_3HN^+ \cdot CF_3CO_2^-$ (a large excess (100 equiv) of TFA was used to generate the *Z*-$H^+$ isomers, and as a result, at least the same amount of $NEt_3$ was added to neutralize the solution). These large amounts of acid and base can significantly change the ionic strength of the solvent and, hence, influence the isomerization rates. These additional kinetic data once again show that, even in the presence of a catalyzing base, the rate measured for **2** ($k_{NEt3}$) is significantly higher than that of **1**, thus lending further support to the involvement of a polar transition state in the isomerization process.

## CONCLUSIONS

We have synthesized and characterized a novel hydrazone-based molecular switch and thoroughly studied the isomerization mechanism of this phenyl-containing system and of a previously reported naphthyl-based one. These unique switches represent the initial steps toward chemically activated configurational rotary switches. The switching process takes place with a change in pH; the *E*-isomer undergoes protonation with TFA that leads to isomerization around the C═N bond. When the protonated compound *Z*-$H^+$ is passed through a plug of $K_2CO_3$ a mixture of isomers (*E* and *Z*) is obtained that equilibrates with time to reinstate the initial isomer ratio. On the other hand $NEt_3$ catalyzes the isomerization process and the *Z* isomer cannot be observed by $^1H$ NMR spectroscopy. The *E*-$H^+$ ↔ *Z*-$H^+$ process was also studied using spectrophotometric methods. The *E* isomer gets protonated in a fast pre-equilibrium to afford the corresponding *E*-$H^+$ kinetic intermediate, which then isomerizes into the more stable *Z*-$H^+$ protonated isomer in a single rate limiting step.

The corresponding kinetic data, and activation parameters, of both the forward and backward isomerization processes demonstrate that the isomerization mechanism involves a polar transition state. Consequently, the isomerization around the C═N double bond *cannot* take place via the lateral inversion mechanism. Thus far, the existence of a polar transition state in these systems was automatically linked to a rotation mechanism around a polar C═N double bond.[24] However, our calculations have shown that hydrazone−azo tautomerization followed by rotation around a C−N single bond is the most likely isomerization mechanism in these H-bonded systems. This mechanism may apply generally to other hydrazones as well.

This study shows that for an accurate determination of the isomerization mechanism in hydrazones, and subsequently imines, it is important to study the contribution of enthalpy and entropy to the Gibbs energy of activation, and not rely solely on isomerization rates. We are currently working on taking advantage of these insights to better tune the performance of these hydrazone-based molecular switches. Now that the nature of the isomerization mechanism has been established, we can use these rotary switches[10] as the basis of molecular rotors and motors that can be incorporated and used in functional materials.[57]

## ASSOCIATED CONTENT

**Supporting Information.** Experimental procedures, NMR spectra of key compounds, UV/vis absorption spectra, kinetic and thermodynamic measurement data, and computational details. These materials are available free of charge via the Internet at http://pubs.acs.org.

## AUTHOR INFORMATION

**Corresponding Author**
ivan.aprahamian@dartmouth.edu

## ACKNOWLEDGMENT

This work was supported by Dartmouth College, the Burke Research Initiation Award, the Centre National de la Recherche Scientifique (CNRS) and the University of Strasbourg (UMR 7509 CNRS-UdS) in France. We thank Wayne T. Casey for the help with NMR spectroscopy and Dr. Richard Staples (Michigan State University) for X-ray analysis. Computational facilities were funded by grants from ARO-DURIP and ONR-DURIP.

## REFERENCES

(1) (a) Feringa, B. L., Ed. *Molecular Switches*; Wiley-VCH: Weinheim, Germany, 2001. (b) Kelly, T. R., Ed. *Top. Curr. Chem.* **2005**, *262*, volume on Molecular Machines. (c) Khuong, T V.; Nunez, J. E.; Godinez, C. E.; Garcia-Garibay, M. A. *Acc. Chem. Res.* **2006**, *39*, 413–422. (d) Kay, E. R.; Leigh, D. A.; Zerbetto, F. *Angew. Chem., Int. Ed.* **2007**, *46*, 72–191. (e) Champin, B.; Mobian, P.; Sauvage, J.-P. *Chem. Soc. Rev.* **2007**, *36*, 358–366. (f) Astumian, R. D. *Phys. Chem. Chem. Phys.* **2007**, *9*, 5067–5083.(g) Balzani, V.; Credi, A.; Venturi, M. *Molecular Devices and Machines: Concepts and Perspectives for the Nanoworld*; Wiley-VCH: Weinheim, Germany, 2008. (h) Vives, G.; Tour, J. M. *Acc. Chem. Res.* **2009**, *42*, 473–487. (i) Stoddart, J. F. *Chem. Soc. Rev.* **2009**, *38*, 1802–1820.

(2) *Molecular Motors*; Schilwa, M., Ed.; Wiley-VCH: Weinheim, Germany, 2003.

(3) (a) Al-Atar, U.; Fernandes, R.; Johnsen, B.; Baillie, D.; Branda, N. R. *J. Am. Chem. Soc.* **2009**, *131*, 15966–15967. (b) Elbaz, J.; Wang, Z.-G.; Orbach, R.; Willner, I. *Nano Lett.* **2009**, *9*, 4510–4514. (c) Silvi, S.; Constable, E. C.; Housecroft, C. E.; Beves, J. E.; Dunphy, E. L.; Tomasulo, M.; Raymo, F. M.; Credi, A. *Chem.—Eur. J.* **2009**, *15*, 178–185. (d) Wang, X.; Zhu, J.; Smithrud, D. B. *J. Org. Chem.* **2010**, *75*, 3358–3370. (e) Gassensmith, J. J.; Matthys, S.; Lee, J.-J.; Wojcik, A.; Kamat, P.; Smith, B. D. *Chem.—Eur. J.* **2010**, *16*, 2916–2921. (f) Davis, J. J.; Orlowski, A. G.; Rahman, H.; Beer, P. D. *Chem. Commun* **2010**, 54–63. (g) Russew, M.-M.; Hecht, S. *Adv. Mater.* **2010**, *22*, 3348–3360.

(4) (a) Amabilino, D. B.; Ashton, P. R.; Balzani, V.; Brown, C. L.; Credi, A.; Frechet, J. M. J.; Leon, J. W.; Raymo, F. M.; Spencer, N.; Stoddart, J. F.; Venturi, M. *J. Am. Chem. Soc.* **1996**, *118*, 12012–12020. (b) Collin, J.; Gavina, P.; Sauvage, J.-P. *New J. Chem.* **1997**, *21*, 525–528. (c) Lane, A. S.; Leigh, D. A.; Murphy, A. *J. Am. Chem. Soc.* **1997**, *119*, 11092–11093. (d) Loeb, S. J.; Wisner, J. A. *Chem. Commun* **2000**, 1939–1940. (e) Brouwer, A. M.; Frochot, C.; Gatti, F. G.; Leigh, D. A.; Mottier, L.; Paolucci, F.; Roffia, S.; Wurpel, G. W. *Science* **2001**, *291*, 2124–2128. (f) Jeppesen, J. O.; Nielsen, K. A.; Perkins, J.; Vignon, S. A.; Di Alberto, F.; Ballardini, R.; Gandolfi, M. T.; Venturi, M.; Balzani, V.; Becher, J.; Stoddart, J. F. *Chem.—Eur. J.* **2003**, *9*, 2982–3007. (g) Badjić, J. D.; Balzani, V.; Credi, A.; Silvi, S.; Stoddart, J. F. *Science* **2004**, *303*, 1845–1849. (h) Kang, S.; Vignon, S. A.; Tseng, H.; Stoddart, J. F. *Chem.—Eur. J.* **2004**, *10*, 2555–2564. (i) Aprahamian, I.; Miljanic, O. S.; Dichtel, W. R.; Isoda, K.; Yasuda, T.; Kato, T.; Stoddart, J. F. *Bull. Chem. Soc. Jpn.* **2007**, *80*, 1856–1869. (j) Durola, F.; Lux, J.; Sauvage, J.-P. *Chem.—Eur. J.* **2009**, *15*, 4124–4134.

(5) (a) Jimenez, M. C.; Dietrich-Buchecker, C.; Sauvage, J.-P. *Angew. Chem., Int. Ed.* **2000**, *39*, 3284–3287. (b) Chiu, S.; Rowan, S. J.; Cantrill, S. J.; Stoddart, J. F.; White, A. J. P.; Williams, D. J. *Chem.—Eur. J.* **2002**, *8*, 5170–5183. (c) Berna, J.; Leigh, D. A.; Lubomska, M.; Mendoza, S. M.; Perez, E. M.; Rudolf, P.; Teobaldi, G.; Francesco, Z. *Nat. Mater.* **2005**, *4*, 704–710. (d) Ebron, V. H.; Yang, Z. W.; Seyer, D. J.; Kozlov, M. E.; Oh, J. Y.; Xie, H.; Razal, J.; Hall, L. J.; Ferraris, J. P.; MacDiarmid, A. G.; Baughman, R. H. *Science* **2006**, *311*, 1580–1583. (e) Stadler, A.; Kyritsakas, N.; Graff, R.; Lehn, J.-M. *Chem.—Eur. J.* **2006**, *12*, 4503–4522. (f) Song, C.; Swager, T. M. *Org. Lett.* **2008**, *10*, 3575–3578. (g) Clark, P. G.; Day, M. W.; Grubbs, R. H. *J. Am. Chem. Soc.* **2009**, *131*, 13631–13633. (h) Juluri, B. K.; Kumar, A. S.; Liu, Y.; Ye, T.; Tang, Y.-W.; Flood, A. H.; Fang, L.; Stoddart, J. F.; Weiss, P. S.; Huang, T. J. *ACS Nano* **2009**, *3*, 291–300. (i) Miwa, K.; Furusho, Y.; Yashima, E. *Nat. Chem.* **2010**, *2*, 444–449.

(6) (a) Chatterjee, M. N.; Kay, E. R.; Leigh, D. A. *J. Am. Chem. Soc.* **2006**, *128*, 4058–4073. (b) Serreli, V.; Lee, C.; Kay, E. R.; Leigh, D. A. *Nature* **2007**, *445*, 523–527. (c) Alvarez-Pérez, M.; Goldup, S. M.; Leigh, D. A.; Slawin, A. M. Z. *J. Am. Chem. Soc.* **2008**, *130*, 1836–1838.

(7) (a) Shin, J.; Pierce, N. A. *J. Am. Chem. Soc.* **2004**, *126*, 10834–10835. (b) Tian, Y.; He, Y.; Chen, Y.; Yin, P.; Mao, C. *Angew. Chem., Int. Ed.* **2005**, *44*, 4355–4358. (c) Yin, P.; Choi, H. M. T.; Calvert, C. R.; Pierce, N. A. *Nature* **2008**, *451*, 318–322. (d) Green, S. J.; Bath, J.; Turberfield, A. J. *Phys. Rev. Lett.* **2008**, *101*, 238101. (e) Omabegho, T.; Sha, R.; Seeman, N. C. *Science* **2009**, *324*, 67–71. (f) von Delius, M.; Geertsema, E. M.; Leigh, D. A. *Nat. Chem.* **2010**, *2*, 96–101.

(8) (a) Gu, H.; Chao, J.; Xiao, S.-J.; Seeman, N. C. *Nature* **2010**, *465*, 202–205. (b) Lund, K.; Manzo, A. J.; Dabby, N.; Michelotti, N.; Johnson-Buck, A.; Nangreave, J.; Taylor, S.; Pei, R.; Stojanovic, M. N.; Walter, N. G.; Winfree, E.; Yan, H. *Nature* **2010**, *465*, 206–210.

(9) (a) Collier, C.; Mattersteig, G.; Wong, E.; Luo, Y.; Beverly, K.; Sampaio, J.; Raymo, F.; Stoddart, J.; Heath, J. R. *Science* **2000**, *289*, 1172–1175. (b) Flood, A.; Stoddart, J.; Steuerman, D.; Heath, J. R. *Science* **2004**, *306*, 2055–2056. (c) Green, J. E.; Choi, J. W.; Boukai, A.; Bunimovich, Y.; Johnston-Halperin, E.; DeIonno, E.; Luo, Y.; Sheriff, B. A.; Xu, K.; Shin, Y. S.; Tseng, H.; Stoddart, J. F.; Heath, J. R. *Nature* **2007**, *445*, 414–417.

(10) Kottas, G. S.; Clarke, L. I.; Horinek, D.; Michl, J. *Chem. Rev.* **2005**, *105*, 1281–1376.

(11) (a) Kelly, T. R.; De Silva, S. H.; Silva, R. A. *Nature* **1999**, *401*, 150–152. (b) Koumura, N.; Zijlstra, R .W.; van Delden, R. A.; Harada, N.; Feringa, B. L. *Nature* **1999**, *401*, 152–155. (c) Leigh, D. A.; Wong, J. K. Y.; Dehez, F.; Zerbetto, F. *Nature* **2003**, *424*, 174–179. (d) Hernández, J. V.; Kay, E. R.; Leigh, D. A. *Science* **2004**, *306*, 1532–1537. (e) Fletcher, S. P.; Dumur, F.; Pollard, M. M.; Feringa, B. L. *Science* **2005**, *310*, 80–82. (f) Lin, Y; Dahl, B. J.; Branchaud, B. P. *Tetrahedron Lett.* **2005**, *46*, 8359–8362. (g) Dahl, B. J.; Branchaud, B. P. *Org. Lett.* **2006**, *8*, 5841–5844. (h) Feringa, B. L. *J. Org. Chem.* **2007**, *72*, 6635–6652. (i) Kelly, T. R.; Cai, X. L.; Damkaci, F.; Panicker, S. B.; Tu, B.; Bushell, S. M.; Cornella, I.; Piggott, M. J.; Salives, R.; Cavero, M.; Zhao, Y.; Jasmin, S. *J. Am. Chem. Soc.* **2007**, *129*, 376–386.

(12) By configuration we mean *cis*−*trans* isomerism around double bonds as suggested by convention. We are distinguishing here between configurational and conformational rotation for the simple fact that energy barriers associated with these two processes are quite different. These differences in isomerization rates can be very important in future applications.

(13) Chaur, M. N.; Collado, D.; Lehn, J.-M. *Chem.—Eur. J.* **2011**, *17*, 248–258.

(14) (a) Vicini, P.; Zani, F.; Cozzini, P.; Doytchinova, I. *Eur. J. Med. Chem.* **2002**, *37*, 553–564. (b) Loncle, C.; Brunel, J.; Vidal, N.; Dherbomez, M.; Letourneux, Y. *Eur. J. Med. Chem.* **2004**, *39*, 1067–1071. (c) Savini, L.; Chiasserini, L.; Travagli, V.; Pellerano, C.; Novellino, E.; Cosentino, S.; Pisano, M. B. *Eur. J. Med. Chem.* **2004**, *39*, 113–122. (d) Cocco, M. T.; Congiu, C.; Lilliu, V.; Onnis, V. *Bioorg. Med. Chem.* **2005**, *14*, 366–372. (e) Masunari, A.; Tavares, L. C. *Bioorg. Med. Chem.* **2007**, *15*, 4229–4236. (f) Vicini, P.; Incerti, M.; La Colla, P.; Loddo, R. *Eur. J. Med. Chem.* **2009**, *44*, 1801–1807.

(15) (a) Rowan, S. J.; Cantrill, S. J.; Cousins, G. R. L.; Sanders, J. K. M.; Stoddart, J. F. *Angew. Chem., Int. Ed.* **2002**, *41*, 898–952. (b) Corbett, P. T.; Leclaire, J.; Vial, L.; West, K. R.; Wietor, J.-L.; Sanders, J. K. M.; Otto, S. *Chem. Rev.* **2006**, *106*, 3652–3711. (c) Lehn, J.-M. *Chem Soc. Rev.* **2007**, *36*, 151–160.(d) Miller, B. L. *Dynamic Combinatorial Chemistry. In Drug Discovery, Bioorganic Chemistry, and Materials Science*; John Wiley & Sons, Inc.: Hoboken, NJ, 2010.

(16) (a) Barboiu, M.; Lehn, J.-M. *Proc. Natl. Acad. Sci. U.S.A.* **2002**, *99*, 5201–5206. (b) Stadler, A.-M.; Kyritsakas, N.; Lehn, J.-M. *Chem. Commun* **2004**, 2024–2025. (c) Hecht, S.; Huc, I., Eds. *Foldamers*; Wiley-VCH: Weinheim, Germany, 2007. (d) Stadler, A.-M.; Ramírez, J.; Lehn, J.-M. *Chem.—Eur. J.* **2010**, *16*, 5369–5378.

(17) (a) Petitjean, A.; Khoury, R. G.; Kyritsakas, N.; Lehn, J.-M. *J. Am. Chem. Soc.* **2004**, *126*, 6637–6647. (b) Ulrich, S.; Petitjean, A.; Lehn, J.-M. *Eur. J. Inorg. Chem.* **2010**, 1913–1928.

(18) McCarthy, C. G. In *The Chemistry of the Carbon-Nitrogen Bond*; Patai, S., Ed.; John Wiley and Sons: New York, 1970; pp 392−399.

(19) Parmerter, S. M. In *Organic Reactions*; Adam, R., Ed.; Wiley-VCH: New York, 1959; Vol. 10, p 1.

(20) (a) Yao, H. C. *J. Org. Chem.* **1964**, *29*, 2959–2963. (b) Bose, A. K.; Kugajevsky, I. *Tetrahedron* **1967**, *23*, 1489–1497. (c) Karabatsos, G. J.; Taller, R. A. *Tetrahedron* **1968**, *24*, 3923–3937. (d) Mitchell, A. D.; Nonhebel, D. C. *Tetrahedron Lett.* **1975**, *16*, 3859–3862. (e) Mitchell, A. D.; Nonhebel, D. C. *Tetrahedron* **1979**, *35*, 2013–2019. (f) Bertolasi, V.; Ferretti, V.; Gilli, P.; Issa, Y. M.; Sherif, O. E. *J. Chem. Soc., Perkin Trans. 2* **1993**, 2223–2228.

(21) (a) Zollinger, H. *Colour Chemistry. Synthesis, Properties and Application of Organic Dyes and Pigments*; VCH: Weinheim, 1991; pp 45−68. (b) Kelemen, J.; Moss, S.; Sauter, H.; Winkler, T. *Dyes Pigm.* **1982**, *3*, 27–47. (c) Hihara, T.; Okada, Y.; Morita, Z. *Dyes Pigm.* **2006**, *69*, 151–176. (d) Lee, H. Y.; Song, X.; Park., H.; Baik, M.-H.; Lee, D. *J. Am. Chem. Soc.* **2010**, *132*, 12133–12144.

(22) (a) Kessler, H. *Tetrahedron* **1974**, *30*, 1861–1870. (b) Padwa, A.; Albrecht, F. *J. Am. Chem. Soc.* **1974**, *96*, 4849–4857. (c) Padwa, A. *Chem. Rev.* **1977**, *77*, 37–68.

(23) (a) Curtin, D. Y.; Grubbs, E. J.; McCarty, C. G. *J. Am. Chem. Soc.* **1966**, *88*, 2775–2786. (b) Kerek, F.; Ostrogovich, G.; Simon, Z. *J. Chem.*

*Soc. B* **1971**, 541–544. (c) Raban, M.; Carlson, E. *J. Am. Chem. Soc.* **1971**, *93*, 685–691. (d) Hall, G. E.; Middleton, W. J.; Roberts, J. D. *J. Am. Chem. Soc.* **1971**, *93*, 4778–4781. (e) Galvez, J.; Guirado, A. *J. Comput. Chem.* **2010**, *31*, 520–531 and references therein.

(24) For examples of the rotation mechanism in hydrazones, please see: (a) Tobin, J. C.; Hegarty, A. F.; Scott, F. L. *J. Chem. Soc. B* **1971**, 2198–2202. (b) Wong, J. L.; Zady, M. F. *J. Org. Chem.* **1975**, *40*, 2512–2516. (c) Pichon, R.; Saint, J.; Le; Courtot, P. *Tetrahedron* **1981**, *37*, 1517–1524.

(25) For examples of the inversion mechanism in hydrazones, please see: (a) Shvo, Y.; Nahlieli, A. *Tetrahedron Lett.* **1970**, *49*, 4273–4274. (b) Kessler, H.; Leibfritz, L. *Liebigs Ann. Chem.* **1970**, *737*, 53–60. (c) Bensai, R.; Taddei, F. *J. Chem. Soc., Perkin Trans. 2* **1985**, 1629–1632. (d) Timpe, H. J.; Mueller, U.; Schuetz, R. *J. Prakt. Chem.* **1986**, *328*, 181–189. (e) Singh, D. K.; Balasubrahmanyam, S. N.; Prasad, N. *Indian J. Chem., Sect. B* **1990**, *29B*, 804–810. (f) Pihlaja, K.; Simeonov, M. F.; Fueloep, F. *J. Org. Chem.* **1997**, *62*, 5080–5088. (g) Srivastava, A.; Srivastava, V.; Verma, S. M. *Indian J. Chem., Sect. B* **1997**, *36B*, 236–241. (h) Ramanathan, S.; Lemal, D. M. *J. Org. Chem.* **2007**, *72*, 1566–1569.

(26) For some examples of conflicting reports on imine isomerization mechanism, please see: (a) Marullo, N. P.; Wagener, E. H. *J. Am. Chem. Soc.* **1966**, *88*, 5034–5035. (b) Vögtle, F.; Mannschr, A.; Staab, H. A. *Justus Liebigs Ann. Chem.* **1967**, *708*, 51–56. (c) Marullo, N. P.; Wagener, E. H. *Tetrahedron Lett.* **1969**, *10*, 2555–2558. (d) Kessler, H.; Leibfritz, L. *Tetrahedron Lett.* **1970**, 1423–1426. (e) Leibfritz, L.; Kessler, H. *Chem. Commun.* **1970**, 655–657.

(27) For some examples of conflicting reports on hydrazone isomerization mechanism, please see ref 25a and: (a) Kalinowski, H.-O.; Kessler, H.; Leibfritz, D.; Pfeffer, A. *Chem. Ber* **1973**, *106*, 1023–1032. (b) Stassinopoulou, C. I.; Zioudrou, C.; Karabatsost, G. J. *Tetrahedron Lett.* **1972**, *13*, 3671–3674. (c) Stassinopoulou, C. I.; Zioudrou, C.; Karabatsost, G. J. *Tetrahedron* **1976**, *32*, 1147–1151. (d) Lu, S.-I. *J. Comput. Chem.* **2009**, *30*, 2176–2180.

(28) (a) Landge, S. M.; Aprahamian, I. *J. Am. Chem. Soc.* **2009**, *131*, 18269–18271. (b) Su, X.; Aprahamian, I. *Org. Lett.* **2011**, *13*, 30–33. (c) Su, X.; Robbins, T. F.; Aprahamian, I. *Angew. Chem., Int. Ed.* **2011**, *50*, 1841–1844.

(29) For some examples of pH activated molecular switches, please see:(a) Dolain, C.; Maurizot, V.; Huc, I. *Angew. Chem., Int. Ed.* **2003**, *42*, 2738–2740. (b) Keaveney, C. M.; Leigh, D. A. *Angew. Chem., Int. Ed.* **2004**, *43*, 1222–1224. (c) Cheng, K.-W.; Lai, C.-C.; Chiang, P.-T.; Chiu, S.-H. *Chem. Commun.* **2006**, 2854–2856. (d) Silvi, S.; Arduini, A.; Pochini, A.; Secchi, A.; Tomasulo, M.; Raymo, F. M.; Baroncini, M.; Credi, A. *J. Am. Chem. Soc.* **2007**, *129*, 13378–13379. (e) Vella, S. J.; Tiburcio, J.; Loeb, S. J. *Chem. Commun.* **2007**, 4752–4754. (f) Silvi, S.; Arduini, A.; Pochini, A.; Secchi, A.; Tomasulo, M.; Raymo, F. M.; Baroncini, M.; Credi, A. *J. Am. Chem. Soc.* **2007**, *129*, 13378–13379. (g) Uchiyama, S.; Iwai, K.; de Silva, A. P. *Angew. Chem., Int. Ed.* **2008**, *47*, 4667–4669. (h) Fang, L.; Hmadeh, M.; Wu, J.; Olson, M. A.; Spruell, J. M.; Trabolsi, A.; Yang, Y.-Y.; Elhabiri, M.; Albrecht-Gary, A.-M.; Stoddart, J. F. *J. Am. Chem. Soc.* **2009**, *131*, 7126–7134. (i) Elbaz, J.; Shimron, S.; Willner, I. *Chem. Commun.* **2010**, 1209–1211. (j) Leblond, J.; Gao, H.; Petitjean, A.; Leroux, J.-C. *J. Am. Chem. Soc.* **2010**, *132*, 8544–8545.

(30) When viewed along the central N−N bond, the torsional angle is −176.73(10)° for **1-*E*** and −179.81(10)° for **2-*E***, and between the $N_{pyr}-C_{pyr}-C_{imin}=N$ atoms it is −3.16(10)° for **1-*E*** and −8.23(10)° for **2-*E***,

(31) These types of hydrazones usually adopt planar structures. For other examples, please see: (a) Vickery, B.; Willey, G. R.; Drew, M. G. B. *J. Chem. Soc., Perkin Trans. 2* **1981**, 155–160. (b) Drew, M. G. B.; Vickery, B.; Willey, G. R. *Acta Crystallogr., Sect. B* **1982**, *38*, 1530–1535. (c) Frohberg, P.; Drutkowski, G.; Wagner, C. *Eur. J. Org. Chem.* **2002**, 1654–1663.

(32) The bond length between the aromatic carbon and the hydrazone nitrogen (N2) is 1.401(1) Å for **1-*E*** and 1.400(1) Å for **2-*E***, and the N(1)−N(2) bond length is 1.321(1) Å for **1-*E*** and 1.326(1) Å for **2-*E***. The length of the imino double bond (C=N) is 1.305(1) Å for **1-*E*** and 1.313(1) Å for **2-*E***.

(33) (a) Kaberia, F.; Vickery, B.; Willey, G. R.; Drew, M. G. B. *J. Chem. Soc., Perkin Trans. 2* **1980**, 1622–1626. (b) Vickery, B.; Willey, G. R.; Drew, M. G. B. *J. Chem. Soc., Perkin Trans. 2* **1981**, 155–160. (c) Vickery, B.; Willey, G. R.; Drew, M. G. B. *J. Chem. Soc., Perkin Trans. 2* **1981**, 1454–1458. (d) Drew, M. G. B.; Vickery, B.; Willey, G. R. *J. Chem. Soc., Perkin Trans. 2* **1982**, 1297–1303. (e) Pavlović, G.; Racané, L.; Čičak, H.; Tralić-Kulenović, V. *Dyes Pigm.* **2009**, *83*, 354–362. (f) Sethukumar, A.; Arul Prakasam, B. *J. Mol. Struct.* **2010**, *963*, 250–257.

(34) (a) Bertolasi, V.; Gilli, P.; Ferretti, V.; Gilli, G. *J. Am. Chem. Soc.* **1991**, *113*, 4917–4925. (b) Bertolasi, V.; Gilli, P.; Ferretti, V.; Gilli, G.; Vaughan, K. *New J. Chem.* **1999**, *23*, 1261–1267. (c) Šimůnek, P.; Svobodová, M.; Bertolasi, V.; Pretto, L.; Lyčka, A.; Macháček, V. *New J. Chem.* **2007**, *31*, 429–438.

(35) The reason for this is most probably the unfavorable *peri* interaction in the other conformation (rotamer).

(36) *Jaguar 7.6 User Manual*, release 110; Schrodinger: New York, 2009.

(37) (a) Zhao, Y.; Truhlar, D. G. *J. Chem. Theory Comput* **2008**, *4*, 1849–1868. (b) Zhao, Y.; Truhlar, D. G. *Theo. Chem. Acc.* **2008**, *120*, 215–241.

(38) Dunning, T .H., Jr. *J. Chem. Phys.* **1989**, *90*, 1007–1023.

(39) Zhao, Y.; Truhlar, D. G. *J. Phys. Chem. A* **2008**, *112*, 6794–6799.

(40) The error in the calculated absolute nuclear magnetic shifts was ~1 ppm. However, the error in the relative nuclear magnetic shifts was observed to be ~0.1 ppm.

(41) Only 1.0 equiv of TFA is needed to fully protonate the starting material, ethyl-2-pyridylacetate. Subsequently, when $CH_3SO_3H$ is used as the acid, only 1.0 equiv is needed to fully protonate the pyridine subunit. It is clear from these data that the H-bond with the hydrazone NH proton is decreasing the basicity of the pyridine nitrogen. We used the kinetic studies (see the equations provided in the UV/vis analysis section) to determine the protonation constant (log $K_H$) of the pyridyl unit in these hydrazone-based systems and found them to be 3.1 ± 0.2 and 2.84 ± 0.2 for **1** and **2**, respectively. These values are comparable, suggesting a weak influence of the aromatic substituents; however, they are significantly lower than the protonation constant of pyridine in $CH_3CN$ ($pK_a$ = 12.33): Kaljurand, I.; Rodima, T.; Leito, I.; Koppel, I. A.; Schwesinger, R. *J. Org. Chem.* **2000**, *65*, 6202–6208.

(42) *Tables of Spectral Data for Structure Determination of Organic Compounds*; Pretsch, E., Ed.; Springer-Verlag: Berlin, Germany, 1989; Vol. 2.

(43) In ethyl-2-pyridylacetate this same proton resonates at 8.50 ppm and shifts to 8.70 ppm upon protonation with TFA. This indicates that the shift to 8.76 ppm in **1-*E*** has to do with the H-bonding and RAHB. In **1-*Z*** the pyridine is not H-bonded, and proton H1 resonates at 8.55 ppm, clearly showing the effect of the H-bond on this proton.

(44) When $NEt_3$ is used as the base, the fully equilibrated spectrum is generated instantaneously, and this process is not observed.

(45) The bond length between (i) the aromatic carbon C(1) and nitrogen N(2) is 1.396(1) Å for **1-*Z*-H$^+$** and 1.395(1) Å for **2-*Z*-H$^+$**); (ii) nitrogens N(2) and N(1) is 1.317(1) Å for **1-*Z*-H$^+$** and 1.319(1) Å for **2-*Z*-H$^+$**; and (iii) the C=N double bond is 1.305(1) Å for **1-*Z*-H$^+$** and 1.301(1) Å for **2-*Z*-H$^+$**, whereas the torsional angle between the $N(1)=C_{imin}-C=O$ atoms is 1.49(10)° for **1-*Z*-H$^+$** and 9.61(10)° for **2-*Z*-H$^+$**.

(46) Regardless of the isomerization or the protonation states of the hydrazone-based switches **1** and **2**, the main absorption of **2** is constantly 10−20% less intense than that of **1**.

(47) It is noteworthy that, at the beginning of the spectrophotometric titrations of **1-*E*** and **2-*E*** by TFA (Figures S15 and S16 in the SI), unexpected spectral variations were observed. These changes were attributed to the initial protonation of the *Z* isomer, which has more basic pyridyl nitrogen, as it is not involved in H-bonding as is the case in the *E* isomer. This observation supports the presence of a mixture of *Z* and *E* isomers in solution, in agreement with the NMR data. The *E* isomers remain by far the predominant species in solution (estimated >95%).

(48) (a) Frost, A. A.; Pearson, R. G. *Kinetics and Mechanism*; John Wiley and Sons, Inc.: New York, NY, 1953. (b) Connors, K. A. *Chemical Kinetics: The Study of Reaction Rates in Solution*; John Wiley and Sons, Inc.: New York, 1990; pp 60−61.

(49) The NMR spectroscopy measurements give $k_{obs}$ which consists of two contributions: $k_{E\rightarrow Z} + k_{Z\rightarrow E}$. The former is faster by 2 orders of magnitude from the latter, and hence, its contribution to $k_{obs}$ is minimal. Therefore, we can assume that $k_{obs} \approx k_{Z\rightarrow E}$. Nevertheless, the $k_{Z\rightarrow E}$ values were used for the different calculations.

(50) The isomerization rate previously reported for **2** in $CD_3CN$ (see ref 28a) was overestimated because base catalysis was not taken into account.

(51) When studying mechanisms that involve polar transition states, it is not enough to only use the dielectric constant values of the solvents in assessing the dependence of rates on solvent polarity. The Dimroth−Reichardt parameter $E_T$ is an empirical measure of solvent polarity, which is based on the solvatochromism of a pyridinium phenoxide. This parameter mainly reflects the electrophilicity and the H-bond donor activity of the solvent and is generally used when intramolecular bonded systems are studied. (a) Dimroth, K.; Reichardt, C.; Siepmann, T.; Bohlmann, F. *Liebigs Ann. Chem.* **1963**, *661*, 1–37. (b) Reichardt, C. *Angew. Chem., Int. Ed.* **1965**, *4*, 29–40. (c) Reichardt, C.; Dimroth, K. *Fortschr. Chem. Forsch.* **1968**, *11*, l–73.

(52) The proposed tautomerization is similar to the one that takes place in 2-pyridone: Wong, M. W.; Wiberg, K. B.; Frisch, M. J. *J. Am. Chem. Soc.* **1992**, *114*, 1645–1652.

(53) Given that the accuracy of our computational method is likely to be around ∼1 kcal/mol, we believe that our calculations are not able to distinguish the difference between the barriers of **1** and **2**.

(54) Reed, A. E.; Curtiss, L. A.; Weinhold, F. *Chem. Rev.* **1988**, *88*, 899–926.Glendening, E. D.; Badenhoop, J, K.; Reed, A. E.; Carpenter, J. E.; Bohmann, J. A.; Morales, C. M.; Weinhold, F. *NBO 5.0*; Theoretical Chemistry Institute, University of Wisconsin: Madison, 2001.

(55) *Biokine, User's Manual*; Bio-Logic Company: Echirolles, France, 1991.

(56) The ordinate at the origin of the fitted curves in Figures S21 and S22 in SI is very close to zero, which means that the backward reaction $Z\text{-}H^+ \rightarrow E\text{-}H^+$ is a very minor process. This makes sense as $E\text{-}H^+$ is most likely an unstable species. Thus, $k_{ZH+\rightarrow EH+} \ll k_{EH+\rightarrow ZH+}$ and so we can assume that $k_{obs} \approx k_{EH+\rightarrow ZH+}$. For this reason we have used $c = 0$ in our calculations.

(57) Michl, J.; Sykes, E. C. H. *ACS Nano* **2009**, 1042–1048.